between elements, and the plane of the rhombus. Rhombic antennas are usually preferred over V's for nonresonant and unidirectional pattern applications because they are less difficult to terminate. Additional directivity and reduction in side lobes can be obtained by stacking, vertically or horizontally, a number of rhombic and/or V antennas to form arrays.

The field radiated by a rhombus can be found by adding the fields radiated by its four legs. For a symmetrical rhombus with equal legs, this can be accomplished using array theory and pattern multiplication. When this is done, a number of design equations can be derived [8]–[11]. For this design, the plane formed by the rhombus is placed parallel and a height h above a perfect electric conductor.

B. Design Equations

Let us assume that it is desired to design a rhombus such that the maximum of the main lobe of the pattern, in a plane which bisects the V of the rhombus, is directed at an angle ψ_0 above the ground plane. The design can be optimized if the height h is selected according to

$$\frac{h_m}{\lambda_0} = \frac{m}{4\cos(90^\circ - \psi_0)}, \quad m = 1, 3, 5, \ldots \tag{10-21}$$

with $m = 1$ representing the minimum height.

The minimum optimum length of each leg of a symmetrical rhombus must be selected according to

$$\frac{l}{\lambda_0} = \frac{0.371}{1 - \sin(90^\circ - \psi_0)\cos\theta_0} \tag{10-22}$$

The best choice for the included angle of the rhombus is selected to satisfy

$$\theta_0 = \cos^{-1}[\sin(90^\circ - \psi_0)] \tag{10-23}$$

10.3 BROADBAND ANTENNAS

In Chapter 9 broadband dipole antennas were discussed. There are numerous other antenna designs that exhibit greater broadband characteristics than those of the dipoles. Some of these antenna can also provide circular polarization, a desired extra feature for many applications. In this section we want to discuss briefly some of the most popular broadband antennas.

10.3.1 Helical Antenna

Another basic, simple, and practical configuration of an electromagnetic radiator is that of a conducting wire wound in the form of a screw thread forming a helix, as shown in Figure 10.13. In most cases the helix is used with a ground plane. The ground plane can take different forms. One is for the ground to be flat, as shown in Figure 10.13. Typically the diameter of the ground plane should be at least $3\lambda/4$. However, the ground plane can also be cupped in the form of a cylindrical cavity (see Figure 10.17) or in the form of a frustrum cavity [8]. In addition, the helix is usually connected to the center conductor of a coaxial transmission line at the feed point with the outer conductor of the line attached to the ground plane.

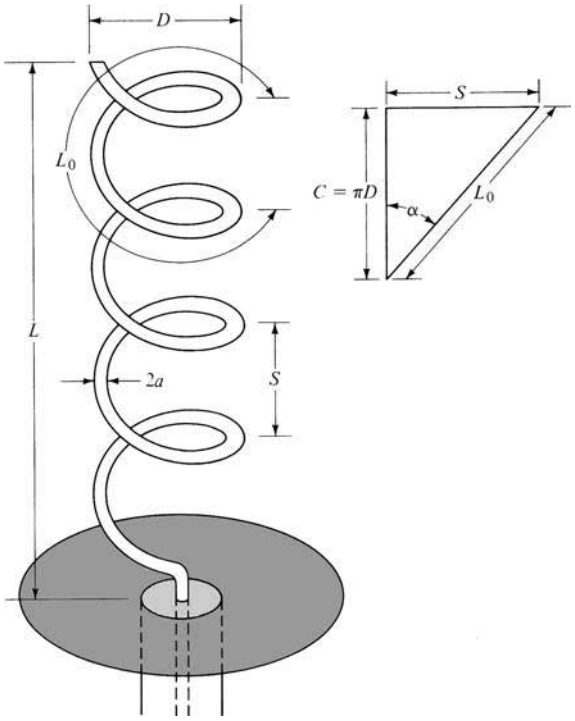

Figure 10.13 Helical antenna with ground plane.

The geometrical configuration of a helix consists usually of N turns, diameter D and spacing S between each turn. The total length of the antenna is $L = NS$ while the total length of the wire is $L_n = NL_0 = N\sqrt{S^2 + C^2}$ where $L_0 = \sqrt{S^2 + C^2}$ is the length of the wire between each turn and $C = \pi D$ is the circumference of the helix. Another important parameter is the pitch angle α which is the angle formed by a line tangent to the helix wire and a plane perpendicular to the helix axis. The pitch angle is defined by

$$\boxed{\alpha = \tan^{-1}\left(\frac{S}{\pi D}\right) = \tan^{-1}\left(\frac{S}{C}\right)} \tag{10-24}$$

When $\alpha = 0^\circ$, then the winding is flattened and the helix reduces to a loop antenna of N turns. On the other hand, when $\alpha = 90^\circ$ then the helix reduces to a linear wire. When $0^\circ < \alpha < 90^\circ$, then a true helix is formed with a circumference greater than zero but less than the circumference when the helix is reduced to a loop ($\alpha = 0^\circ$).

The radiation characteristics of the antenna can be varied by controlling the size of its geometrical properties compared to the wavelength. The input impedance is critically dependent upon the pitch angle and the size of the conducting wire, especially near the feed point, and it can be adjusted by controlling their values. The general polarization of the antenna is elliptical. However circular and linear polarizations can be achieved over different frequency ranges.

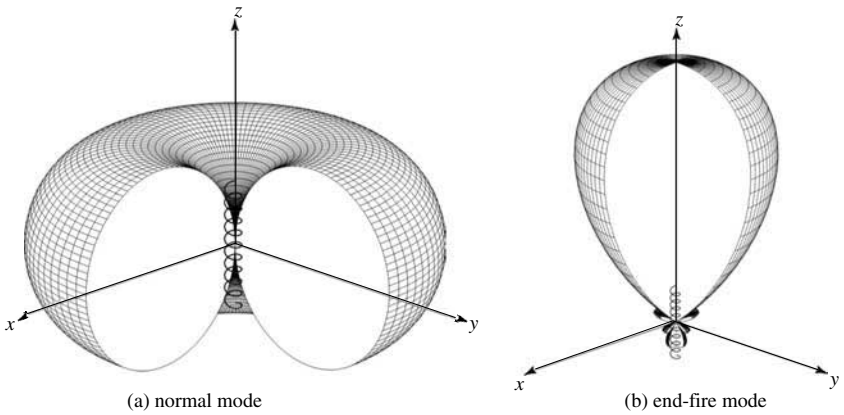

Figure 10.14 Three-dimensional normalized amplitude linear power patterns for *normal* and *end-fire* modes helical designs.

The helical antenna can operate in many modes; however the two principal ones are the *normal* (*broadside*) and the *axial* (*end-fire*) modes. The three-dimensional amplitude patterns representative of a helix operating, respectively, in the normal (broadside) and axial (end-fire) modes are shown in Figure 10.14. The one representing the normal mode, Figure 10.14(a), has its maximum in a plane normal to the axis and is nearly null along the axis. The pattern is similar in shape to that of a small dipole or circular loop. The pattern representative of the axial mode, Figure 10.14(b), has its maximum along the axis of the helix, and it is similar to that of an end-fire array. More details are in the sections that follow. The axial (end-fire) mode is usually the most practical because it can achieve circular polarization over a wider bandwidth (usually 2:1) and it is more efficient.

Because an elliptically polarized antenna can be represented as the sum of two orthogonal linear components in time-phase quadrature, a helix can always receive a signal transmitted from a rotating linearly polarized antenna. Therefore helices are usually positioned on the ground for space telemetry applications of satellites, space probes, and ballistic missiles to transmit or receive signals that have undergone Faraday rotation by traveling through the ionosphere.

A. Normal Mode

In the normal mode of operation the field radiated by the antenna is maximum in a plane normal to the helix axis and minimum along its axis, as shown sketched in Figure 10.14(a), which is a figure-eight rotated about its axis similar to that of a linear dipole of $l < \lambda_0$ or a small loop ($a \ll \lambda_0$). To achieve the normal mode of operation, the dimensions of the helix are usually small compared to the wavelength (i.e., $NL_0 \ll \lambda_0$).

The geometry of the helix reduces to a loop of diameter D when the pitch angle approaches zero and to a linear wire of length S when it approaches 90°. Since the limiting geometries of the helix are a loop and a dipole, the far field radiated by a small helix in the normal mode can be described in terms of E_θ and E_ϕ components of the dipole and loop, respectively. In the normal mode, the helix of Figure 10.15(a) can

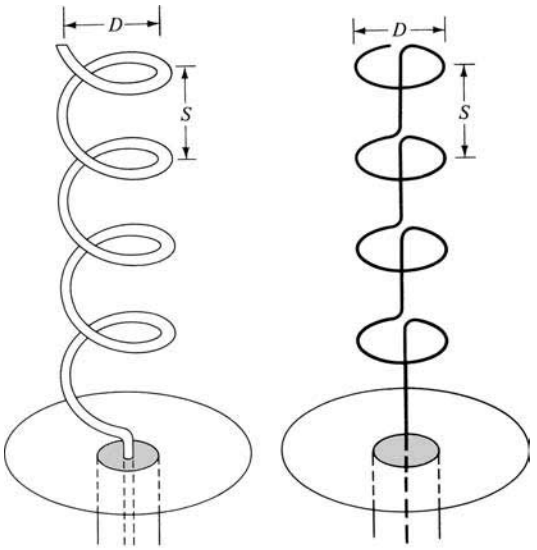

Figure 10.15 Normal (broadside) mode for helical antenna and its equivalent.

be simulated approximately by N small loops and N short dipoles connected together in series as shown in Figure 10.14(b). The fields are obtained by superposition of the fields from these elemental radiators. The planes of the loops are parallel to each other and perpendicular to the axes of the vertical dipoles. The axes of the loops and dipoles coincide with the axis of the helix.

Since in the normal mode the helix dimensions are small, the current throughout its length can be assumed to be constant and its relative far-field pattern to be independent of the number of loops and short dipoles. Thus its operation can be described accurately by the sum of the fields radiated by a small loop of radius D and a short dipole of length S, with its axis perpendicular to the plane of the loop, and each with the same constant current distribution.

The far-zone electric field radiated by a short dipole of length S and constant current I_0 is E_θ, and it is given by (4-26a) as

$$E_\theta = j\eta \frac{kI_0 S e^{-jkr}}{4\pi r} \sin\theta \tag{10-25}$$

where l is being replaced by S. In addition the electric field radiated by a loop is E_ϕ, and it is given by (5-27b) as

$$E_\phi = \eta \frac{k^2 (D/2)^2 I_0 e^{-jkr}}{4r} \sin\theta \tag{10-26}$$

where $D/2$ is substituted for a. A comparison of (10-25) and (10-26) indicates that the two components are in time-phase quadrature, a necessary but not sufficient condition for circular or elliptical polarization.

The ratio of the magnitudes of the E_θ and E_ϕ components is defined here as the axial ratio (AR), and it is given by

$$\boxed{\text{AR} = \frac{|E_\theta|}{|E_\phi|} = \frac{4S}{\pi k D^2} = \frac{2\lambda S}{(\pi D)^2}} \tag{10-27}$$

By varying the D and/or S the axial ratio attains values of $0 \leq \text{AR} \leq \infty$. The value of $\text{AR} = 0$ is a special case and occurs when $E_\theta = 0$ leading to a linearly polarized wave of horizontal polarization (the helix is a loop). When $\text{AR} = \infty$, $E_\phi = 0$ and the radiated wave is linearly polarized with vertical polarization (the helix is a vertical dipole). Another special case is the one when AR is unity ($\text{AR} = 1$) and occurs when

$$\frac{2\lambda_0 S}{(\pi D)^2} = 1 \tag{10-28}$$

or

$$\boxed{C = \pi D = \sqrt{2S\lambda_0}} \tag{10-28a}$$

for which

$$\boxed{\tan\alpha = \frac{S}{\pi D} = \frac{\pi D}{2\lambda_0}} \tag{10-29}$$

When the dimensional parameters of the helix satisfy the above relation, the radiated field is circularly polarized in *all directions* other than $\theta = 0^\circ$ where the fields vanish.

When the dimensions of the helix do not satisfy any of the above special cases, the field radiated by the antenna is not circularly polarized. The progression of polarization change can be described geometrically by beginning with the pitch angle of zero degrees ($\alpha = 0^\circ$), which reduces the helix to a loop with linear horizontal polarization. As α increases, the polarization becomes elliptical with the major axis being horizontally polarized. When α, is such that $C/\lambda_0 = \sqrt{2S/\lambda_0}$, $\text{AR} = 1$ and we have circular polarization. For greater values of α, the polarization again becomes elliptical but with the major axis vertically polarized. Finally when $\alpha = 90^\circ$ the helix reduces to a linearly polarized vertical dipole.

To achieve the normal mode of operation, it has been assumed that the current throughout the length of the helix is of constant magnitude and phase. This is satisfied to a large extent provided the total length of the helix wire NL_0 is very small compared to the wavelength ($L_n \ll \lambda_0$) and its end is terminated properly to reduce multiple reflections. Because of the critical dependence of its radiation characteristics on its geometrical dimensions, which must be very small compared to the wavelength, this mode of operation is very narrow in bandwidth and its radiation efficiency is very small. Practically this mode of operation is limited, and it is seldom utilized.

B. Axial Mode

A more practical mode of operation, which can be generated with great ease, is the axial or end-fire mode. In this mode of operation, there is only one major lobe and its

maximum radiation intensity is along the axis of the helix, as shown in Figure 10.14(b). The minor lobes are at oblique angles to the axis.

To excite this mode, the diameter D and spacing S must be large fractions of the wavelength. To achieve circular polarization, primarily in the major lobe, the circumference of the helix must be in the $\frac{3}{4} < C/\lambda_0 < \frac{4}{3}$ range (with $C/\lambda_0 = 1$ near optimum), and the spacing about $S \simeq \lambda_0/4$. The pitch angle is usually $12^\circ \leq \alpha \leq 14^\circ$. Most often the antenna is used in conjunction with a ground plane, whose diameter is at least $\lambda_0/2$, and it is fed by a coaxial line. However, other types of feeds (such as waveguides and dielectric rods) are possible, especially at microwave frequencies. The dimensions of the helix for this mode of operation are not as critical, thus resulting in a greater bandwidth.

C. Design Procedure

The terminal impedance of a helix radiating in the axial mode is nearly resistive with values between 100 and 200 ohms. Smaller values, even near 50 ohms, can be obtained by properly designing the feed. Empirical expressions, based on a large number of measurements, have been derived [8], and they are used to determine a number of parameters. The input impedance (purely resistive) is obtained by

$$\boxed{R \simeq 140\left(\frac{C}{\lambda_0}\right)} \tag{10-30}$$

which is accurate to about $\pm 20\%$, the half-power beamwidth by

$$\boxed{\text{HPBW (degrees)} \simeq \frac{52\lambda_0^{3/2}}{C\sqrt{NS}}} \tag{10-31}$$

the beamwidth between nulls by

$$\boxed{\text{FNBW (degrees)} \simeq \frac{115\lambda_0^{3/2}}{C\sqrt{NS}}} \tag{10-32}$$

the directivity by

$$\boxed{D_0 \text{ (dimensionless)} \simeq 15N\frac{C^2S}{\lambda_0^3}} \tag{10-33}$$

the axial ratio (for the condition of increased directivity) by

$$\boxed{\text{AR} = \frac{2N+1}{2N}} \tag{10-34}$$

and the normalized far-field pattern by

$$E = \sin\left(\frac{\pi}{2N}\right)\cos\theta\frac{\sin[(N/2)\psi]}{\sin[\psi/2]} \tag{10-35}$$

where

$$\psi = k_0\left(S\cos\theta - \frac{L_0}{p}\right) \tag{10-35a}$$

$$p = \frac{L_0/\lambda_0}{S/\lambda_0 + 1} \qquad \text{For ordinary end-fire radiation} \tag{10-35b}$$

$$p = \frac{L_0/\lambda_0}{S/\lambda_0 + \left(\dfrac{2N+1}{2N}\right)} \qquad \text{For Hansen-Woodyard end-fire radiation} \tag{10-35c}$$

All these relations are approximately valid provided $12^\circ < \alpha < 14^\circ$, $\frac{3}{4} < C/\lambda_0 < \frac{4}{3}$, and $N > 3$.

The far-field pattern of the helix, as given by (10-35), has been developed by assuming that the helix consists of an array of N identical turns (each of nonuniform current and identical to that of the others), a uniform spacing S between them, and the elements are placed along the z-axis. The $\cos\theta$ term in (10-35) represents the field pattern of a single turn, and the last term in (10-35) is the array factor of a uniform array of N elements. The total field is obtained by multiplying the field from one turn with the array factor (pattern multiplication).

The value of p in (10-35a) is the ratio of the velocity with which the wave travels along the helix wire to that in free space, and it is selected according to (10-35b) for ordinary end-fire radiation or (10-35c) for Hansen-Woodyard end-fire radiation. These are derived as follows.

For ordinary end-fire the relative phase ψ among the various turns of the helix (elements of the array) is given by (6-7a), or

$$\psi = k_0 S\cos\theta + \beta \tag{10-36}$$

where $d = S$ is the spacing between the turns of the helix. For an end-fire design, the radiation from each one of the turns along $\theta = 0^\circ$ must be in phase. Since the wave along the helix wire between turns travels a distance L_0 with a wave velocity $v = pv_0$ ($p < 1$ where v_0 is the wave velocity in free space) and the desired maximum radiation is along $\theta = 0^\circ$, then (10-36) for *ordinary end-fire* radiation is equal to

$$\psi = (k_0 S\cos\theta - kL_0)_{\theta=0^\circ} = k_0\left(S - \frac{L_0}{p}\right) = -2\pi m, \quad m = 0, 1, 2, \ldots \tag{10-37}$$

Solving (10-37) for p leads to

$$p = \frac{L_0/\lambda_0}{S/\lambda_0 + m} \tag{10-38}$$

For $m = 0$ and $p = 1$, $L_0 = S$. This corresponds to a straight wire ($\alpha = 90°$), and not a helix. Therefore the next value is $m = 1$, and it corresponds to the first transmission mode for a helix. Substituting $m = 1$ in (10-38) leads to

$$p = \frac{L_0/\lambda_0}{S/\lambda_0 + 1} \tag{10-38a}$$

which is that of (10-35b).

In a similar manner, it can be shown that for Hansen-Woodyard end-fire radiation (10-37) is equal to

$$\psi = (k_0 S \cos\theta - kL_0)_{\theta=0°} = k_0\left(S - \frac{L_0}{p}\right) = -\left(2\pi m + \frac{\pi}{N}\right), \quad m = 0, 1, 2, \ldots \tag{10-39}$$

which when solved for p leads to

$$p = \frac{L_0/\lambda_0}{S/\lambda_0 + \left(\dfrac{2mN + 1}{2N}\right)} \tag{10-40}$$

For $m = 1$, (10-40) reduces to

$$p = \frac{L_0/\lambda_0}{S/\lambda_0 + \left(\dfrac{2N + 1}{2N}\right)} \tag{10-40a}$$

which is identical to (10-35c).

Example 10.1

Design a 10-turn helix to operate in the axial mode. For an optimum design,

1. Determine the:
   a. Circumference (in λ_o), pitch angle (*in degrees*), and separation between turns (in λ_o)
   b. Relative (to free space) wave velocity along the wire of the helix for:
      i. Ordinary end-fire design
      ii. Hansen-Woodyard end-fire design
   c. Half-power beamwidth of the main lobe (*in degrees*)
   d. Directivity (in dB) using:
      i. A formula
      ii. The computer program ***Directivity*** of Chapter 2
   e. Axial ratio (*dimensionless* and in *dB*)
2. Plot the normalized three-dimensional linear power pattern for the ordinary and Hansen-Woodyard designs.

Solution:

1. a. For an optimum design

$$C \simeq \lambda_o, \alpha \simeq 13^\circ \Rightarrow S = C\tan\alpha = \lambda_o \tan(13^\circ) = 0.231\lambda_o$$

b. The length of a single turn is

$$L_o = \sqrt{S^2 + C^2} = \lambda_o\sqrt{(0.231)^2 + (1)^2} = 1.0263\lambda_o$$

Therefore the relative wave velocity is:

i. Ordinary end-fire:

$$p = \frac{v_h}{v_o} = \frac{L_o/\lambda_o}{S_o/\lambda_o + 1} = \frac{1.0263}{0.231 + 1} = 0.8337$$

ii. Hansen-Woodyard end-fire:

$$p = \frac{v_h}{v_o} = \frac{L_o/\lambda_o}{S_o/\lambda_o + \left(\dfrac{2N+1}{2N}\right)} = \frac{1.0263}{0.231 + 21/20} = 0.8012$$

c. The half-power beamwidth according to (10-31) is

$$\text{HPBW} \simeq \frac{52\lambda_o^{3/2}}{C\sqrt{NS}} = \frac{52}{1\sqrt{10(0.231)}} = 34.2135^\circ$$

d. The directivity is:

i. Using (10-33):

$$D_o \simeq 15N\frac{C^2S}{\lambda_o^3} = 15(10)(1)^2(0.231) = 34.65 \text{ (}\textit{dimensionless}\text{)}$$

$$= 15.397 \text{ dB}$$

ii. Using the computer program ***Directivity*** and (10-35):

a. ordinary end-fire ($p = 0.8337$): $D_o = 12.678$ (*dimensionless*)

$$= 11.03 \text{ dB}$$

b. H-W end-fire ($p = 0.8012$): $D_o = 26.36$ (*dimensionless*) $= 14.21$ dB

e. The axial ratio according to (10-34) is:

$$\text{AR} = \frac{2N+1}{2N} = \frac{20+1}{20} = 1.05 \text{ (}\textit{dimensionless}\text{)} = 0.21 \text{ dB}$$

2. The three-dimensional linear power patterns for the two end-fire designs, *ordinary* and *Hansen-Woodyard*, are shown in Figure 10.16.

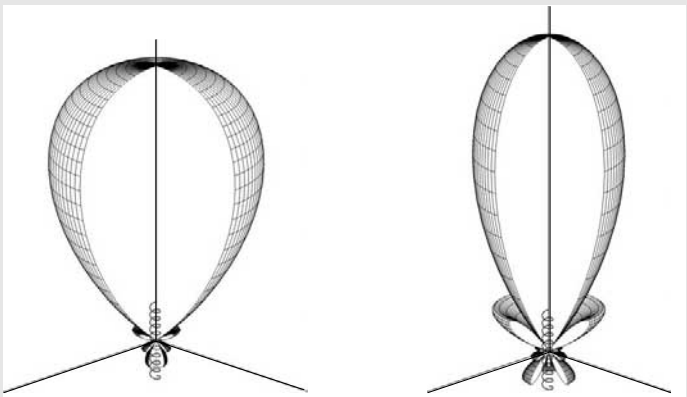

(a) ordinary end-fire (b) Hansen-Woodyard end-fire

Figure 10.16 Three-dimensional normalized amplitude linear power patterns for helical *ordinary* ($p = 0.8337$) and *Hansen-Woodyard* ($p = 0.8012$) end-fire designs.

D. Feed Design

The nominal impedance of a helical antenna operating in the axial mode, computed using (10-30), is 100–200 ohms. However, many practical transmission lines (such as a coax) have characteristic impedance of about 50 ohms. In order to provide a better match, the input impedance of the helix must be reduced to near that value. There may be a number of ways by which this can be accomplished. One way to effectively control the input impedance of the helix is to properly design the first 1/4 turn of the helix which is next to the feed [8], [12]. To bring the input impedance of the helix from nearly 150 ohms down to 50 ohms, the wire of the first 1/4 turn should be flat in the form of a strip and the transition into a helix should be very gradual. This is accomplished by making the wire from the feed, at the beginning of the formation of the helix, in the form of a strip of width w by flattening it and nearly touching the ground plane which is covered with a dielectric slab of height [2]

$$h = \frac{w}{\dfrac{377}{\sqrt{\epsilon_r} Z_0} - 2} \tag{10-41}$$

where

w = width of strip conductor of the helix starting at the feed
ϵ_r = dielectric constant of the dielectric slab covering the ground plane
Z_0 = characteristic impedance of the input transmission line

Typically the strip configuration of the helix transitions from the strip to the regular circular wire and the designed pitch angle of the helix very gradually within the first 1/4–1/2 turn.

This modification decreases the characteristic impedance of the conductor-ground plane effective transmission line, and it provides a lower impedance over a substantial

but reduced bandwidth. For example, a 50-ohm helix has a VSWR of less than 2:1 over a 40% bandwidth compared to a 70% bandwidth for a 140-ohm helix. In addition, the 50-ohm helix has a VSWR of less than 1.2:1 over a 12% bandwidth as contrasted to a 20% bandwidth for one of 140 ohms.

A simple and effective way of increasing the thickness of the conductor near the feed point will be to bond a thin metal strip to the helix conductor [12]. For example, a metal strip 70-mm wide was used to provide a 50-ohm impedance in a helix whose conducting wire was 13-mm in diameter and it was operating at 230.77 MHz.

A commercially available helix with a cupped ground plane is shown in Figure 10.17. It is right-hand circularly-polarized (RHCP) operating between 100–160 MHz with a gain of about 6 dB at 100 MHz and 12.8 dB at 160 MHz. The right-hand winding of the wire is clearly shown in the photo. The axial ratio is about 8 dB at 100 MHz and 2 dB at 160 MHz. The maximum VSWR in the stated operating frequency, relative to a 50-ohm line, does not exceed 3:1.

A MATLAB computer program, entitled ***Helix***, has been developed to analyze and design a helical antenna. The description of the program is found in the corresponding READ ME file included in the CD attached to the book.

10.3.2 Electric-Magnetic Dipole

It has been shown in the previous section that the circular polarization of a helical antenna operating in the normal mode was achieved by assuming that the geometry of the helix is represented by a number of horizontal small loops and vertical infinitesimal dipoles. It would then seem reasonable that an antenna with only one loop and a single vertical dipole would, in theory, represent a radiator with an elliptical polarization. Ideally circular polarization, in all space, can be achieved if the current in each element can be controlled, by dividing the available power between the dipole and the loop, so that the magnitude of the field intensity radiated by each is equal.

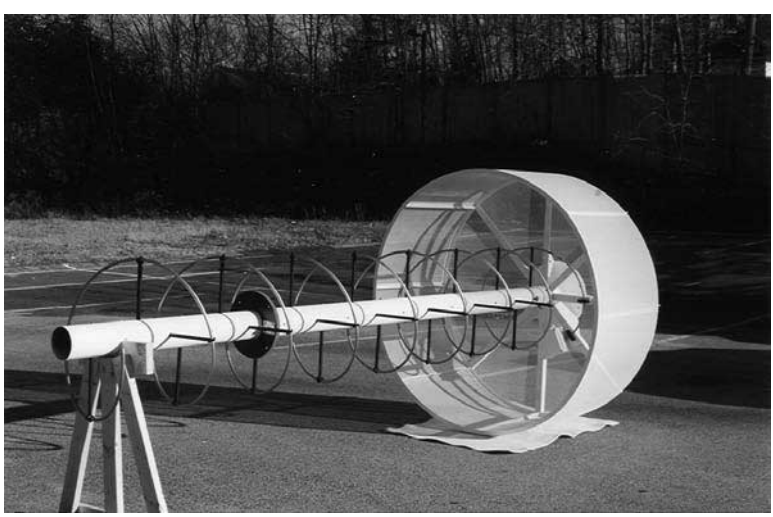

Figure 10.17 Commercial helix with a cupped ground plane. (Courtesy: Seavey Engineering Associates, Inc, Pembroke, MA).

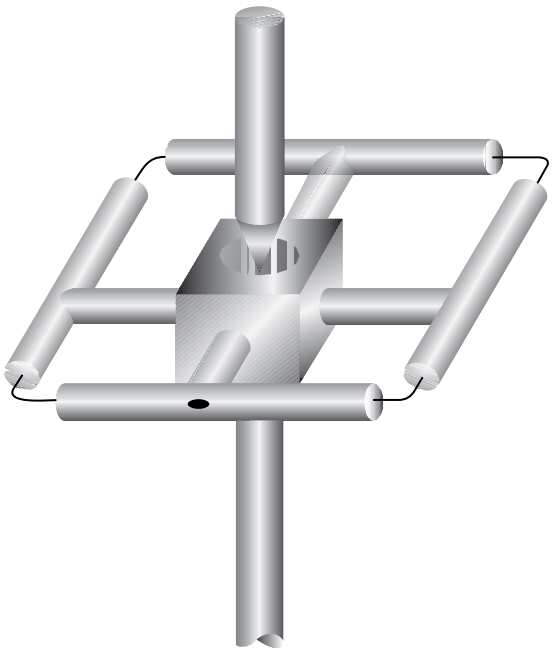

Figure 10.18 Electric-magnetic dipole configuration. (SOURCE: A. G. Kandoian, "Three New Antenna Types and Their Applications," *Proc. IRE*, Vol. 34, pp. 70W–75W, February 1946. © (1946) IEEE).

Experimental models of such an antenna were designed and built [13] one operating around 350 MHz and the other near 1.2 GHz. A sketch of one of them is shown in Figure 10.18. The measured VSWR in the 1.15–1.32 GHz frequency range was less than 2:1.

This type of an antenna is very useful in UHF communication networks where considerable amount of fading may exist. In such cases the fading of the horizontal and vertical components are affected differently and will not vary in the same manner. Hopefully, even in severe cases, there will always be one component all the time which is being affected less than the other, thus providing continuous communication. The same results would apply in VHF and/or UHF broadcasting. In addition, a transmitting antenna of this type would also provide the versatility to receive with horizontally or vertically polarized elements, providing a convenience in the architectural design of the receiving station.

10.3.3 Yagi-Uda Array of Linear Elements

Another very practical radiator in the HF (3–30 MHz), VHF (30–300 MHz), and UHF (300–3,000 MHz) ranges is the Yagi-Uda antenna. This antenna consists of a number of linear dipole elements, as shown in Figure 10.19, one of which is energized directly by a feed transmission line while the others act as parasitic radiators whose currents are induced by mutual coupling. A common feed element for a Yagi-Uda antenna is a folded dipole. This radiator is exclusively designed to operate as an end-fire array, and it is accomplished by having the parasitic elements in the forward beam act as

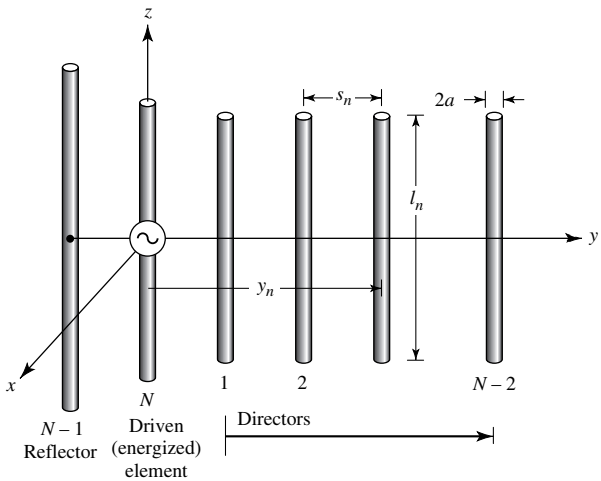

Figure 10.19 Yagi-Uda antenna configuration.

directors while those in the rear act as reflectors. Yagi designated the row of directors as a "wave canal." The Yagi-Uda array has been widely used as a home TV antenna; so it should be familiar to most of the readers, if not to the general public.

The original design and operating principles of this radiator were first described in Japanese in articles published in the Journal of I.E.E. of Japan by S. Uda of the Tohoku Imperial University in Japan [14]. In a later, but more widely circulated and read article [15], one of Professor Uda's colleagues, H. Yagi, described the operation of the same radiator in English. This paper has been considered a classic, and it was reprinted in 1984 in its original form in the *Proceedings of the IEEE* [15] as part of IEEE's centennial celebration. Despite the fact that Yagi in his English written paper acknowledged the work of Professor Uda on beam radiators at a wavelength of 4.4 m, it became customary throughout the world to refer to this radiator as a *Yagi* antenna, a generic term in the antenna dictionary. However, in order for the name to reflect more appropriately the contributions of both inventors, it should be called a *Yagi-Uda* antenna, a name that will be adopted in this book. Although the work of Uda and Yagi was done in the early 1920s and published in the middle 1920s, full acclaim in the United States was not received until 1928 when Yagi visited the United States and presented papers at meetings of the Institute of Radio Engineers (IRE) in New York, Washington, and Hartford. In addition, his work was published in the *Proceedings of IRE*, June 1928, where J. H. Dellinger, Chief of Radio Division, Bureau of Standards, Washington, D.C., and himself a pioneer of radio waves, characterized it as "exceptionally fundamental" and wrote "I have never listened to a paper that I felt so sure was destined to be a classic." So true!!

In 1984, IEEE celebrated its centennial year (1884–1984). Actually, IEEE was formed in 1963 when the IRE and AIEE united to form IEEE. During 1984, the *Proceedings of the IEEE* republished some classic papers, in their original form, in the different areas of electrical engineering that had appeared previously either in the *Proceeding of the IRE* or *IEEE*. In antennas, the only paper that was republished was that by Yagi [15]. Not only that, in 1997, the *Proceedings of the IEEE* republished for the second time the original paper by Yagi [15], [16]. That in itself tells us something

of the impact this particular classic antenna design had on the electrical engineering profession.

The Yagi-Uda antenna has received exhaustive analytical and experimental investigations in the open literature and elsewhere. It would be impractical to list all the contributors, many of whom we may not be aware. However, we will attempt to summarize the salient point of the analysis, describe the general operation of the radiator, and present some design data.

To achieve the end-fire beam formation, the parasitic elements in the direction of the beam are somewhat smaller in length than the feed element. Typically the driven element is resonant with its length slightly less than $\lambda/2$ (usually $0.45-0.49\lambda$) whereas the lengths of the directors should be about 0.4 to 0.45λ. However, the directors are not necessarily of the same length and/or diameter. The separation between the directors is typically 0.3 to 0.4λ, and it is not necessarily uniform for optimum designs. It has been shown experimentally that for a Yagi-Uda array of 6λ total length the overall gain was independent of director spacing up to about 0.3λ. A significant drop (5–7 dB) in gain was noted for director spacings greater than 0.3λ. For that antenna, the gain was also independent of the radii of the directors up to about 0.024λ. The length of the reflector is somewhat greater than that of the feed. In addition, the separation between the driven element and the reflector is somewhat smaller than the spacing between the driven element and the nearest director, and it is found to be near optimum at 0.25λ.

Since the length of each director is smaller than its corresponding resonant length, the impedance of each is capacitive and its current leads the induced emf. Similarly the impedances of the reflectors is inductive and the phases of the currents lag those of the induced emfs. The total phase of the currents in the directors and reflectors is not determined solely by their lengths but also by their spacing to the adjacent elements. Thus, properly spaced elements with lengths slightly less than their corresponding resonant lengths (less than $\lambda/2$) act as directors because they form an array with currents approximately equal in magnitude and with equal progressive phase shifts which will reinforce the field of the energized element toward the directors. Similarly, a properly spaced element with a length of $\lambda/2$ or slightly greater will act as a reflector. Thus a Yagi-Uda array may be regarded as a structure supporting a traveling wave whose performance is determined by the current distribution in each element and the phase velocity of the traveling wave. It should be noted that the previous discussion on the lengths of the directors, reflectors, and driven elements is based on the first resonance. Higher resonances are available near lengths of λ, $3\lambda/2$, and so forth, but are seldom used.

In practice, the major role of the reflector is played by the first element next to the one energized, and very little in the performance of a Yagi-Uda antenna is gained if more than one (at the most two) elements are used as reflectors. However, considerable improvements can be achieved if more directors are added to the array. Practically there is a limit beyond which very little is gained by the addition of more directors because of the progressive reduction in magnitude of the induced currents on the more extreme elements. Usually most antennas have about 6 to 12 directors. However, many arrays have been designed and built with 30 to 40 elements. Array lengths on the order of 6λ have been mentioned [17] as typical. A gain (relative to isotropic) of about 5 to 9 per wavelength is typical for such arrays, which would make the overall gain on the order of about 30 to 54 (14.8–17.3 dB) typical.

The radiation characteristics that are usually of interest in a Yagi-Uda antenna are the *forward and backward gains, input impedance, bandwidth, front-to-back ratio*, and *magnitude of minor lobes*. The lengths and diameters of the directors and reflectors, as well as their respective spacings, determine the optimum characteristics. For a number of years optimum designs were accomplished experimentally. However, with the advent of high-speed computers many different numerical techniques, based on analytical formulations, have been utilized to derive the geometrical dimensions of the array for optimum operational performance. Usually Yagi-Uda arrays have low input impedance and relatively narrow bandwidth (on the order of about 2%). Improvements in both can be achieved at the expense of others (such as gain, magnitude of minor lobes, etc.). Usually a compromise is made, and it depends on the particular design. One way to increase the input impedance without affecting the performance of other parameters is to use an impedance step-up element as a feed (such as a two-element folded dipole with a step-up ratio of about 4). Front-to-back ratios of about 30 ($\simeq$15 dB) can be achieved at wider than optimum element spacings, but they usually are compromised somewhat to improve other desirable characteristics.

The Yagi-Uda array can be summarized by saying that its performance can be considered in three parts:

1. the reflector-feeder arrangement
2. the feeder
3. the rows of directors

It has been concluded, numerically and experimentally, that the reflector spacing and size have (1) negligible effects on the forward gain and (2) large effects on the backward gain (front-to-back ratio) and input impedance, and they can be used to control or optimize antenna parameters without affecting the gain significantly. The feeder length and radius has a small effect on the forward gain but a large effect on the backward gain and input impedance. Its geometry is usually chosen to control the input impedance that most commonly is made real (resonant element). The size and spacing of the directors have a large effect on the forward gain, backward gain, and input impedance, and they are considered to be the most critical elements of the array.

Yagi-Uda arrays are quite common in practice because they are lightweight, simple to build, low-cost, and provide moderately desirable characteristics (including a unidirectional beam) for many applications. The design for a small number of elements (typically five or six) is simple but the design becomes quite critical if a large number of elements are used to achieve a high directivity. To increase the directivity of a Yagi-Uda array or to reduce the beamwidth in the E-plane, several rows of Yagi-Uda arrays can be used [18] to form a *curtain* antenna. To neutralize the effects of the feed transmission line, an odd number of rows is usually used.

A. Theory: Integral Equation-Moment Method

There have been many experimental [19], [20] investigations and analytical [21]–[30] formulations of the Yagi-Uda array. A method [25] based on rigorous integral equations for the electric field radiated by the elements in the array will be presented and it will be used to describe the complex current distributions on all the elements, the phase

velocity, and the corresponding radiation patterns. The method is similar to that of [25], which is based on Pocklington's integral equation of (8-24) while the one presented here follows that of [25] but is based on Pocklington's integral equation of (8-22) and formulated by Tirkas [26]. Mutual interactions are also included and, in principle, there are no restrictions on the number of elements. However, for computational purposes, point-matching numerical methods, based on the techniques of Section 8.4, are used to evaluate and satisfy the integral equation at discrete points on the axis of each element rather than everywhere on the surface of every element. The number of discrete points where boundary conditions are matched must be sufficient in number to allow the computed data to compare well with experimental results.

The theory is based on Pocklington's integral equation of (8-22) for the total field generated by an electric current source radiating in an unbounded free-space, or

$$\int_{-l/2}^{+l/2} I(z')\left(\frac{\partial^2}{\partial z^2}+k^2\right)\frac{e^{-jkR}}{R}dz' = j4\pi\omega\epsilon_0 E_z^t \tag{10-42}$$

where

$$R=\sqrt{(x-x')^2+(y-y')^2+(z-z')^2} \tag{10-42a}$$

Since

$$\frac{\partial^2}{\partial z^2}\left(\frac{e^{-jkR}}{R}\right)=\frac{\partial^2}{\partial z'^2}\left(\frac{e^{-jkR}}{R}\right) \tag{10-43}$$

(10-42) reduces to

$$\int_{-l/2}^{+l/2} I(z')\frac{\partial^2}{\partial z'^2}\left(\frac{e^{-jkR}}{R}\right)dz' + k^2\int_{-l/2}^{+l/2} I(z')\frac{e^{-jkR}}{R}dz' = j4\pi\omega\epsilon_0 E_z^t \tag{10-44}$$

We will now concentrate in the integration of the first term of (10-44). Integrating the first term of (10-44) by parts where

$$u = I(z') \tag{10-45}$$

$$du = \frac{dI(z')}{dz'}dz' \tag{10-45a}$$

$$dv = \frac{\partial^2}{\partial z'^2}\left(\frac{e^{-jkR}}{R}\right)dz' = \frac{\partial}{\partial z'}\left[\frac{\partial}{\partial z'}\left(\frac{e^{-jkR}}{R}\right)\right]dz' \tag{10-46}$$

$$v = \frac{\partial}{\partial z'}\left(\frac{e^{-jkR}}{R}\right) \tag{10-46a}$$

reduces it to

$$\int_{-l/2}^{+l/2} I(z')\frac{\partial^2}{\partial z'^2}\left(\frac{e^{-jkR}}{R}\right)dz' = I(z')\left[\frac{\partial}{\partial z'}\left(\frac{e^{-jkR}}{R}\right)\right]\Bigg|_{-l/2}^{+l/2} - \int_{-l/2}^{+l/2}\frac{\partial}{\partial z'}\left(\frac{e^{-jkR}}{R}\right)\frac{dI(z')}{dz'}dz' \tag{10-47}$$

Since we require that the current at the ends of each wire vanish [i.e., $I_z(z' = +l/2) = I_z(z' = -l/2) = 0$], (10-47) reduces to

$$\int_{-l/2}^{+l/2} I(z') \frac{\partial^2}{\partial z'^2} \left(\frac{e^{-jkR}}{R} \right) dz' = - \int_{-l/2}^{+l/2} \frac{\partial}{\partial z'} \left(\frac{e^{-jkR}}{R} \right) dz' \frac{dI(z')}{dz'} \tag{10-48}$$

Integrating (10-48) by parts where

$$u = \frac{dI(z')}{dz'} \tag{10-49}$$

$$du = \frac{d^2 I(z')}{dz'^2} dz' \tag{10-49a}$$

$$dv = \frac{\partial}{\partial z'} \left(\frac{e^{-jkR}}{R} \right) dz' \tag{10-50}$$

$$v = \frac{e^{-jkR}}{R} \tag{10-50a}$$

reduces (10-48) to

$$\int_{-l/2}^{+l/2} I(z') \frac{\partial^2}{\partial z'^2} \left(\frac{e^{-jkR}}{R} \right) dz' = - \frac{dI(z')}{dz'} \frac{e^{-jkR}}{R} \Bigg|_{-l/2}^{+l/2} + \int_{-l/2}^{+l/2} \frac{d^2 I(z')}{dz'^2} \frac{e^{-jkR}}{R} dz' \tag{10-51}$$

When (10-51) is substituted for the first term of (10-44) reduces it to

$$- \frac{dI(z')}{dz'} \frac{e^{-jkR}}{R} \Bigg|_{-l/2}^{+l/2} + \int_{-l/2}^{+l/2} \left[k^2 I(z') + \frac{d^2 I(z')}{dz'^2} \right] \frac{e^{-jkR}}{R} dz' = j4\pi\omega\epsilon_0 E_z^t \tag{10-52}$$

For small diameter wires the current on each element can be approximated by a finite series of odd-ordered even modes. Thus, the current on the nth element can be written as a Fourier series expansion of the form [26]

$$I_n(z') = \sum_{m=1}^{M} I_{nm} \cos \left[(2m-1) \frac{\pi z'}{l_n} \right] \tag{10-53}$$

where I_{nm} represents the complex current coefficient of mode m on element n and l_n represents the corresponding length of the n element. Taking the first and second derivatives of (10-53) and substituting them, along with (10-53), into (10-52) reduces it to

$$\sum_{m=1}^{M} I_{nm} \left\{ \frac{(2m-1)\pi}{l_n} \sin \left[(2m-1) \frac{\pi z_n'}{l_n} \right] \frac{e^{-jkR}}{R} \Bigg|_{-l_n/2}^{+l_n/2} + \left[k^2 - \frac{(2m-1)^2 \pi^2}{l_n^2} \right] \times \int_{-l_n/2}^{+l_n/2} \cos \left[(2m-1) \frac{\pi z_n'}{l_n} \right] \frac{e^{-jkR}}{R} dz_n' \right\} = j4\pi\omega\epsilon_0 E_z^t \tag{10-54}$$

Since the cosine is an even function, (10-54) can be reduced by integrating over only $0 \le z' \le l/2$ to

$$\sum_{m=1}^{M} I_{nm} \left\{ (-1)^{m+1} \frac{(2m-1)\pi}{l_n} G_2\left(x, x', y, y'/z, \frac{l_n}{2}\right) + \left[k^2 - \frac{(2m-1)^2\pi^2}{l_n^2}\right] \times \int_0^{l_n/2} G_2(x, x', y, y'/z, z_n') \cos\left[\frac{(2m-1)\pi z_n'}{l_n}\right] dz_n' \right\} = j4\pi\omega\epsilon_0 E_z^t \tag{10-55}$$

where

$$G_2(x, x', y, y'/z, z_n') = \frac{e^{-jkR_-}}{R_-} + \frac{e^{-jkR_+}}{R_+} \tag{10-55a}$$

$$R_\pm = \sqrt{(x-x')^2 + (y-y')^2 + a^2 + (z \pm z')^2} \tag{10-55b}$$

$n = 1, 2, 3, \ldots, N$
$N =$ total number of elements

where

$R_\pm$ is the distance from the center of each wire radius to the center of any other wire, as shown in Figure 10.20(a).

The integral equation of (10-55) is valid for each element, and it assumes that the number M of current modes is the same for each element. To apply the Moment Method solution to the integral equation of (10-55), each wire element is subdivided in M segments. On each element, other than the driven element, the matching is done at the center of the wire, and it requires that E_z^t of (10-55) vanishes at each matching point of each segment [i.e., $E_z^t(z = z_i) = 0$], as shown in Figure 10.20(b). On the driven element the matching is done on the surface of the wire, and it requires that E_z^t of (10-55) vanishes at $M - 1$ points, even though there are m modes, and it excludes the segment at the feed as shown in Figure 10.20(c). This generates $M - 1$ equations. The Mth equation on the feed element is generated by the constraint that the normalized current for all M modes at the feed point ($z' = 0$) of the driven element is equal to unity [25], [27], or

$$\sum_{m=1}^{M} I_{nm}(z' = 0)\Big|_{n=N} = 1 \tag{10-56}$$

Based on the above procedure, a system of linear equations is generated by taking into account the interaction of

a. each mode in each wire segment with each segment on the same wire.
b. each mode in each wire segment with each segment on the other wires.

This system of linear equations is then solved to find the complex amplitude coefficients of the current distribution in each wire as represented by (10-53). This is demonstrated in [25] for a three-element array (one director, one reflector, and the driven element) with two modes in each wire.

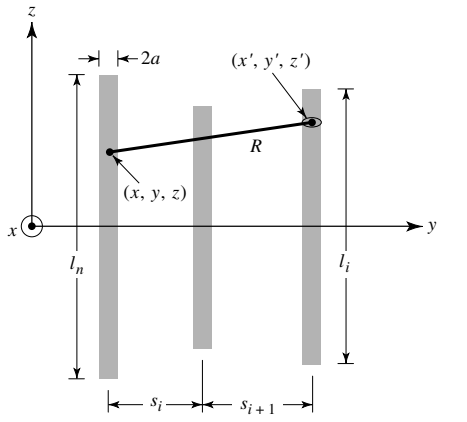

(a) Separation distance

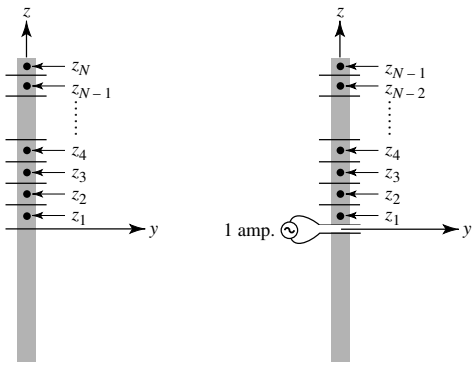

(b) Parasitic elements (c) Driven element

Figure 10.20 Geometry of Yagi-Uda array for Moment Method formulation (SOURCE: G. A. Thiele, "Yagi-Uda Type Antennas," *IEEE Trans. Antennas Propagat.*, Vol. AP-17, No. 1, pp. 24–31, January 1969. © (1969) IEEE).

B. Far-Field Pattern

Once the current distribution is found, the far-zone field generated by each element can be found using the techniques outlined in Chapter 3. The total field of the entire Yagi-Uda array is obtained by summing the contributions from each.

Using the procedure outlined in Chapter 3, Section 3.6, the far-zone electric field generated by the M modes of the nth element oriented parallel to the z axis is given by

$$E_{\theta n} \simeq -j\omega A_{\theta n} \tag{10-57}$$

$$A_{\theta n} \simeq -\frac{\mu e^{-jkr}}{4\pi r}\sin\theta \int_{-l_n/2}^{+l_n/2} I_n e^{jk(x_n \sin\theta\cos\phi + y_n \sin\theta \sin\phi + z_n' \cos\theta)}\, dz_n'$$

$$\simeq -\frac{\mu e^{-jkr}}{4\pi r}\sin\theta \left[e^{jk(x_n \sin\theta\cos\phi + y_n \sin\theta\sin\phi)} \int_{-l_n/2}^{+l_n/2} I_n e^{jkz_n' \cos\theta}\, dz_n' \right] \tag{10-57a}$$

where x_n, y_n represent the position of the nth element. The total field is then obtained by summing the contributions from each of the N elements, and it can be written as

$$E_\theta = \sum_{n=1}^{N} E_{\theta n} = -j\omega A_\theta \tag{10-58}$$

$$A_\theta = \sum_{n=1}^{N} A_{\theta n} = -\frac{\mu e^{-jkr}}{4\pi r}\sin\theta \sum_{n=1}^{N}\left\{ e^{jk(x_n \sin\theta\cos\phi + y_n \sin\theta \sin\phi)} \times \left[\int_{-l_n/2}^{+l_n/2} I_n e^{jkz_n' \cos\theta}\, dz_n'\right]\right\} \tag{10-58a}$$

For each wire, the current is represented by (10-53). Therefore the last integral in (10-58a) can be written as

$$\int_{-l_n/2}^{+l_n/2} I_n e^{jkz_n' \cos\theta} dz_n' = \sum_{m=1}^{M} I_{nm} \int_{-l_n/2}^{+l_n/2} \cos\left[\frac{(2m-1)\pi z_n'}{l_n}\right] e^{jkz_n' \cos\theta} dz_n' \tag{10-59}$$

Since the cosine is an even function, (10-59) can also be expressed as

$$\begin{aligned}\int_{-l_n/2}^{+l_n/2} I_n e^{jkz_n' \cos\theta}\, dz_n' &= \sum_{m=1}^{M} I_{nm} \int_{0}^{+l_n/2} 2\cos\left[\frac{(2m-1)\pi z_n'}{l_n}\right] \\ &\quad \times \left[\frac{e^{jkz_n' \cos\theta} + e^{-jkz_n' \cos\theta}}{2}\right] dz_n' \\ &= \sum_{m=1}^{M} I_{nm} \int_{0}^{+l_n/2} 2\cos\left[\frac{(2m-1)\pi z_n'}{l_n}\right] \\ &\quad \times \cos(kz_n' \cos\theta) dz_n'\end{aligned} \tag{10-60}$$

Using the trigonometric identity

$$2\cos(\alpha)\cos(\beta) = \cos(\alpha+\beta) + \cos(\alpha-\beta) \tag{10-61}$$

(10-60) can be rewritten as

$$\begin{aligned}\int_{-l_n/2}^{+l_n/2} I_n e^{jkz_n' \cos\theta}\, dz_n' &= \sum_{m=1}^{M} I_{nm} \left\{ \int_{0}^{+l_n/2} \cos\left[\frac{(2m-1)\pi}{l_n} + k\cos\theta\right] z_n'\, dz_n' \right. \\ &\quad \left. + \int_{0}^{+l_n/2} \cos\left[\frac{(2m-1)\pi}{l_n} - k\cos\theta\right] z_n'\, dz_n' \right\}\end{aligned} \tag{10-62}$$

Since

$$\int_0^{\alpha/2} \cos[(b \pm c)z]\, dz = \frac{\alpha}{2}\frac{\sin\left[(b \pm c)\frac{\alpha}{2}\right]}{(b \pm c)\frac{\alpha}{2}} \tag{10-63}$$

(10-62) can be reduced to

$$\int_{-l_n/2}^{+l_n/2} I_n e^{jkz'_n \cos\theta}\, dz'_n = \sum_{m=1}^{M} I_{nm} \left[\frac{\sin(Z^+)}{Z^+} + \frac{\sin(Z^-)}{Z^-} \right] \frac{l_n}{2} \tag{10-64}$$

$$Z^+ = \left[\frac{(2m-1)\pi}{l_n} + k\cos\theta \right] \frac{l_n}{2} \tag{10-64a}$$

$$Z^- = \left[\frac{(2m-1)\pi}{l_n} - k\cos\theta \right] \frac{l_n}{2} \tag{10-64b}$$

Thus, the total field represented by (10-58) and (10-58a) can be written as

$$E_\theta = \sum_{n=1}^{N} E_{\theta n} = -j\omega A \tag{10-65}$$

$$A_\theta = \sum_{n=1}^{N} A_{\theta n} = -\frac{\mu e^{-jkr}}{4\pi r} \sin\theta \sum_{n=1}^{N} \left\{ e^{jk(x_n \sin\theta\cos\phi + y_n \sin\theta \sin\phi)} \times \sum_{m=1}^{M} I_{nm} \left[\frac{\sin(Z^+)}{Z^+} + \frac{\sin(Z^-)}{Z^-} \right] \right\} \frac{l_n}{2} \tag{10-65a}$$

There have been other analyses [28], [29] based on the integral equation formulation that allows the conversion to algebraic equations. In order not to belabor further the analytical formulations, which in call cases are complicated because of the antenna structure, it is appropriate at this time to present some results and indicate design procedures.

C. Computer Program and Results

Based on the preceding formulation, a MATLAB and FORTRAN computer program entitled ***Yagi_Uda*** has been developed [26] that computes the E- and H-plane patterns, their corresponding half-power beamwidths, and the directivity of the Yagi-Uda array. The program is described in the corresponding READ ME file, and both are included in the CD attached to the book. The input parameters include the total number of elements (N), the number of current modes in each element (M), the length of each element, and the spacing between the elements. The program assumes one reflector, one driven element, and $N-2$ directors. For the development of the formulation and computer program, the numbering system ($n = 1, 2, \ldots, N$) for the elements begins with the first director ($n = 1$), second director ($n = 2$), etc. The reflector is represented by the next to the last element ($n = N-1$), while the driven element is designated as the last element ($n = N$), as shown in Figure 10.19.

One Yagi-Uda array design is considered here, which is the same as one of the two included in [25]; the other ones are assigned as end of the chapter problems. The patterns, beamwidths, and directivities were computed based on the computer program developed here.

Example 10.2

Design a Yagi-Uda array of 15 elements (13 directors, one reflector, and the exciter). Compute and plot the E- and H-plane patterns, normalized current at the center of each element, and directivity and front-to-back ratio as a function of reflector spacing and director spacing. Use the computer program ***Yagi_Uda*** of this chapter. The dimensions of the array are as follows:

$$N = \text{total number of elements} = 15$$
$$\text{number of directors} = 13$$
$$\text{number of reflectors} = 1$$
$$\text{number of exciters} = 1$$
$$\text{total length of reflector} = 0.5\lambda$$
$$\text{total length of feeder} = 0.47\lambda$$
$$\text{total length of each director} = 0.406\lambda$$
$$\text{spacing between reflector and feeder} = 0.25\lambda$$
$$\text{spacing between adjacent directors} = 0.34\lambda$$
$$a = \text{radius of wires} = 0.003\lambda$$

Solution: Using the computer program of this chapter, the computed E- and H-plane patterns of this design are shown in Figure 10.21. The corresponding beamwidths are: E-plane ($\Theta_e = 26.98^\circ$), H-plane ($\Theta_h = 27.96^\circ$) while the directivity is 14.64 dB. A plot of the current at the center of each element versus position of the element is shown in Figure 10.22; the current of the feed element at its center is unity, as required by (10-56). One important *figure-of-merit* in Yagi-Uda array is the *front-to-back* ratio of the pattern $[20\log_{10} E(\theta = 90^\circ, \phi = 90^\circ)/E(\theta = 90^\circ, \phi = 270^\circ)]$ as a function of the spacing of the reflector with respect to the feeder. This, along with the directivity, is shown in Figure 10.23 for spacing from $0.1\lambda - 0.5\lambda$. For this design, the maximum front-to-back ratio occurs for a reflector spacing of about 0.23λ while the directivity is monotonically decreasing very gradually, from about 15.2 dB at a spacing of 0.1λ down to about 10.4 dB at a spacing of 0.5λ.

Another important parametric investigation is the variation of the front-to-back ratio and directivity as a function of director spacing. This is shown in Figure 10.24 for spacings from 0.1λ to 0.5λ. It is apparent that the directivity exhibits a slight increase from about 12 dB at a spacing of about 0.1λ to about 15.3 dB at a spacing of about 0.45λ. A steep drop in directivity occurs for spacings greater than about 0.45λ. This agrees with the conclusion arrived at in [19] and [28] that large reductions in directivity occur in Yagi-Uda array designs for spacings greater than about 0.4λ. For this design, the variations of the front-to-back ratio are much more sensitive as a function of director spacing, as shown in Figure 10.24; excursions on the order of 20–25 dB are evident for changes in spacing of about 0.05λ. Such variations in front-to-back ratio as shown in Figure 10.24, as a function of director spacing, are not evident in Yagi-Uda array designs with a smaller number of elements. However, they are even more pronounced for designs with a larger number of elements. Both of these are demonstrated in design problems assigned at the end of the chapter.

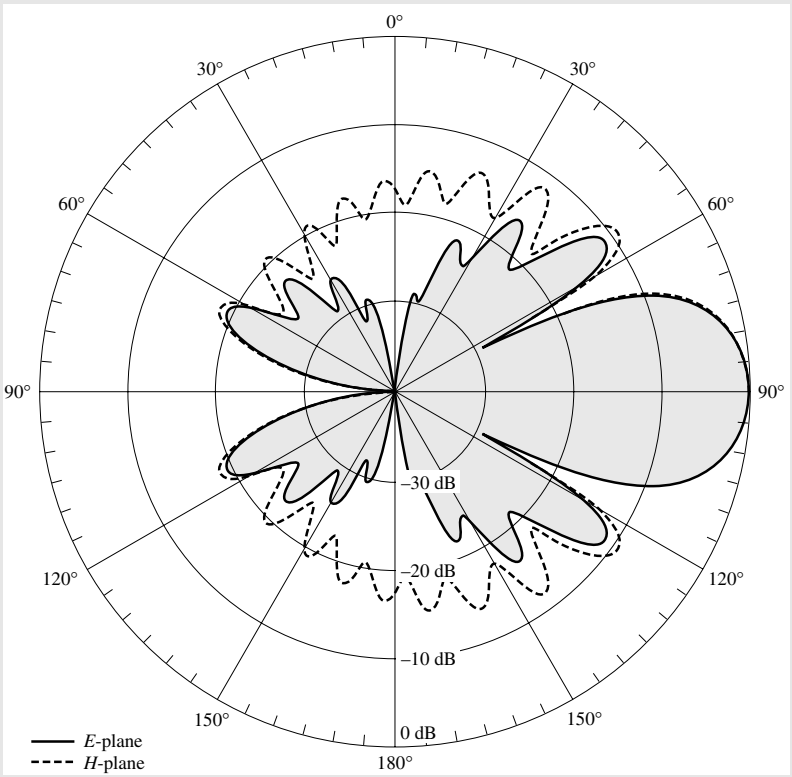

Figure 10.21 *E*- and *H*-plane amplitude patterns of 15-element Yagi-Uda array.

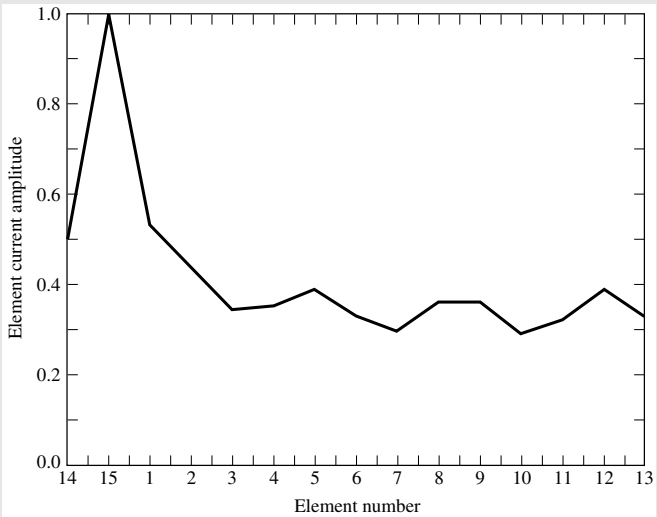

Figure 10.22 Normalized current at the center of each element of a 15-element Yagi-Uda array.

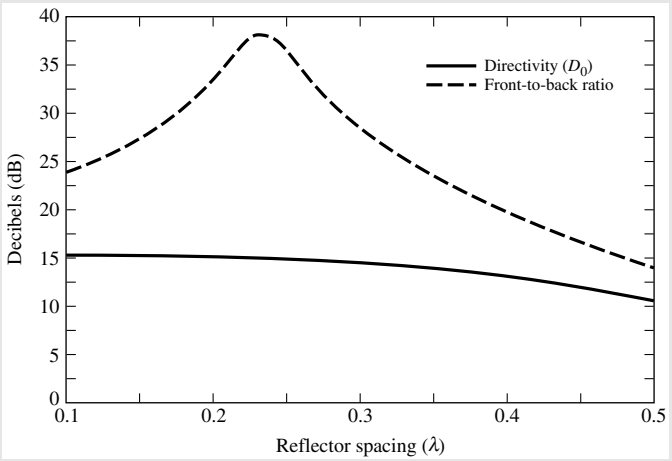

Figure 10.23 Directivity and front-to-back ratio, as a function of reflector spacing, of a 15-element Yagi-Uda array.

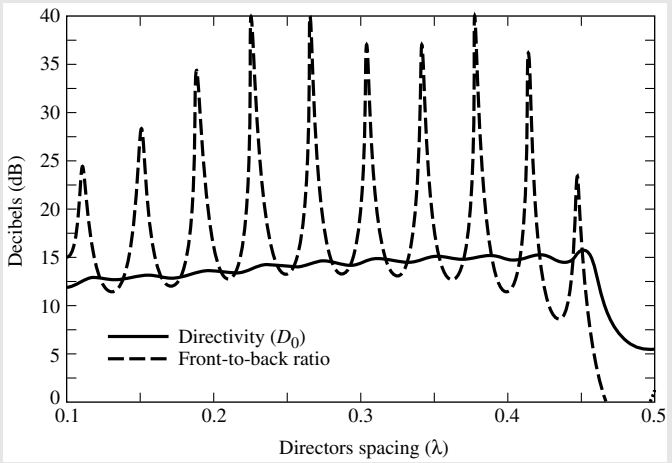

Figure 10.24 Directivity and front-to-back ratio, as a function of director spacing, for 15-element Yagi-Uda array.

D. Optimization

The radiation characteristics of the array can be adjusted by controlling the geometrical parameters of the array. This was demonstrated in Figures 10.23 and 10.24 for the 15-element array using uniform lengths and making uniform variations in spacings. However, these and other array characteristics can be optimized by using nonuniform director lengths and spacings between the directors. For example, the spacing between the directors can be varied while holding the reflector–exciter spacing and the lengths of all elements constant. Such a procedure was used by Cheng and Chen [28] to optimize the directivity of a six-element (four-director, reflector, exciter) array using

TABLE 10.1 Directivity Optimization for Six-Element Yagi-Uda Array (Perturbation of *Director Spacings*), $l_1 = 0.51\lambda$, $l_2 = 0.50\lambda$, $l_3 = l_4 = l_5 = l_6 = 0.43\lambda$, $a = 0.003369\lambda$

	s_{21}/λ	s_{32}/λ	s_{43}/λ	s_{54}/λ	s_{65}/λ	Directivity (dB)
Initial array	0.250	0.310	0.310	0.310	0.310	11.21
Optimized array	0.250	0.336	0.398	0.310	0.407	12.87

(SOURCE: D. K. Cheng and C. A. Chen, "Optimum Spacings for Yagi-Uda Arrays," *IEEE Trans. Antennas Propag.*, Vol. AP-21, pp. 615–623, September 1973. © (1973) IEEE).

TABLE 10.2 Directivity Optimization for Six-Element Yagi-Uda Array (Perturbation of *All Element Spacings*), $l_1 = 0.51\lambda$, $l_2 = 0.50\lambda$, $l_3 = l_4 = l_5 = l_6 = 0.43\lambda$, $a = 0.003369\lambda$

	s_{21}/λ	s_{32}/λ	s_{43}/λ	s_{54}/λ	s_{65}/λ	Directivity (dB)
Initial array	0.280	0.310	0.310	0.310	0.310	10.92
Optimized array	0.250	0.352	0.355	0.354	0.373	12.89

(SOURCE: D. K. Cheng and C. A. Chen, "Optimum Spacings for Yagi-Uda Arrays," *IEEE Trans. Antennas Propag.*, Vol. AP-21, pp. 615–623, September 1973. © (1973) IEEE).

a perturbational technique. The results of the initial and the optimized (perturbed) array are shown in Table 10.1. For the same array, they allowed all the spacings to vary while maintaining constant all other parameters. The results are shown in Table 10.2.

Another optimization procedure is to maintain the spacings between all the elements constant and vary the lengths so as to optimize the directivity. The results of a six-element array [29] are shown in Table 10.3. The ultimate optimization is to vary both the spacings and lengths. This was accomplished by Chen and Cheng [29] whereby they first optimized the array by varying the spacing, while maintaining the lengths constant. This was followed, on the same array, with perturbations in the lengths while maintaining the optimized spacings constant. The results of this procedure are shown in Table 10.4 with the corresponding H-plane ($\theta = \pi/2, \phi$) far-field patterns shown in Figure 10.25. In all, improvements in directivity and front-to-back ratio are noted. The ideal optimization will be to allow the lengths and spacings to vary simultaneously. Such an optimization was not performed in [28] or [29], although it could have been done iteratively by repeating the procedure.

TABLE 10.3 Directivity Optimization for Six-Element Yagi-Uda Array (Perturbation of *All Element Lengths*), $s_{21} = 0.250\lambda$, $s_{32} = s_{43} = s_{54} = s_{65} = 0.310\lambda$, $a = 0.003369\lambda$

	l_1/λ	l_2/λ	l_3/λ	l_4/λ	l_5/λ	l_6/λ	Directivity (dB)
Initial array	0.510	0.490	0.430	0.430	0.430	0.430	10.93
Length-perturbed array	0.472	0.456	0.438	0.444	0.432	0.404	12.16

(SOURCE: C. A. Chen and D. K. Cheng, "Optimum Element Lengths for Yagi-Uda Arrays," *IEEE Trans. Antennas Propag.*, Vol. AP-23, pp. 8–15, January 1975. © (1975) IEEE).

TABLE 10.4 Directivity Optimization for Six-Element Yagi-Uda Array (Perturbation of *Director Spacings and All Element Lengths*), $a = 0.003369\lambda$

	l_1/λ	l_2/λ	l_3/λ	l_4/λ	l_5/λ	l_6/λ	s_{21}/λ	s_{32}/λ	s_{43}/λ	s_{54}/λ	s_{65}/λ	Directivity (dB)
Initial array	0.510	0.490	0.430	0.430	0.430	0.430	0.250	0.310	0.310	0.310	0.310	10.93
Array after spacing perturbation	0.510	0.490	0.430	0.430	0.430	0.430	0.250	0.289	0.406	0.323	0.422	12.83
Optimum array after spacing and length perturbation	0.472	0.452	0.436	0.430	0.434	0.430	0.250	0.289	0.406	0.323	0.422	13.41

(SOURCE: C. A. Chen and D. K. Cheng, "Optimum Element Lengths for Yagi-Uda Arrays," *IEEE Trans. Antennas Propag*., Vol. AP-23, pp. 8–15, January 1975. © (1975) IEEE).

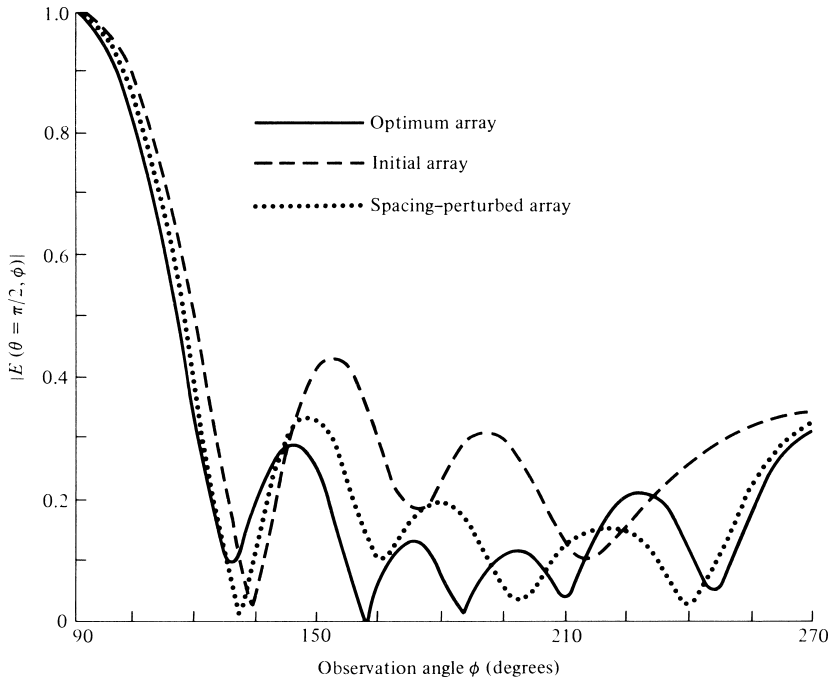

Figure 10.25 Normalized amplitude antenna patterns of initial, perturbed, and optimum six-element Yagi-Uda arrays (Table 10.4). (SOURCE: C. A. Chen and D. K. Cheng, "Optimum Element Lengths for Yagi-Uda Arrays," *IEEE Trans. Antennas Propagat.*, Vol. AP-23, pp. 8–15, January 1975. © (1975) IEEE).

Another parameter that was investigated for the directivity-optimized Yagi-Uda antenna was the frequency bandwidth [30]. The results of such a procedure are shown in Figure 10.26. The antenna was a six-element array optimized at a center frequency f_0. The array was designed, using space perturbations on all the elements, to yield an optimum directivity at f_0. The geometrical parameters are listed in Table 10.2. The 3-dB bandwidth seems to be almost the same for the initial and the optimized arrays. The rapid decrease in the directivity of the initial and optimized arrays at frequencies higher than f_0 and nearly constant values below f_0 may be attributed to the structure of the antenna which can support a "traveling wave" at $f < f_0$ but not at $f > f_0$. It has thus been suggested that an increase in the bandwidth can be achieved if the geometrical dimensions of the antenna are chosen slightly smaller than the optimum.

E. Input Impedance and Matching Techniques

The input impedance of a Yagi-Uda array, measured at the center of the driven element, is usually small and it is strongly influenced by the spacing between the reflector and feed element. For a 13-element array using a resonant driven element, the measured input impedances are listed in Table 10.5 [22]. Some of these values are low for matching to a 50-, 78-, or 300-ohm transmission lines.

There are many techniques that can be used to match a Yagi-Uda array to a transmission line and eventually to the receiver, which in many cases is a television set which has a large impedance (on the order of 300 ohms). Two common matching

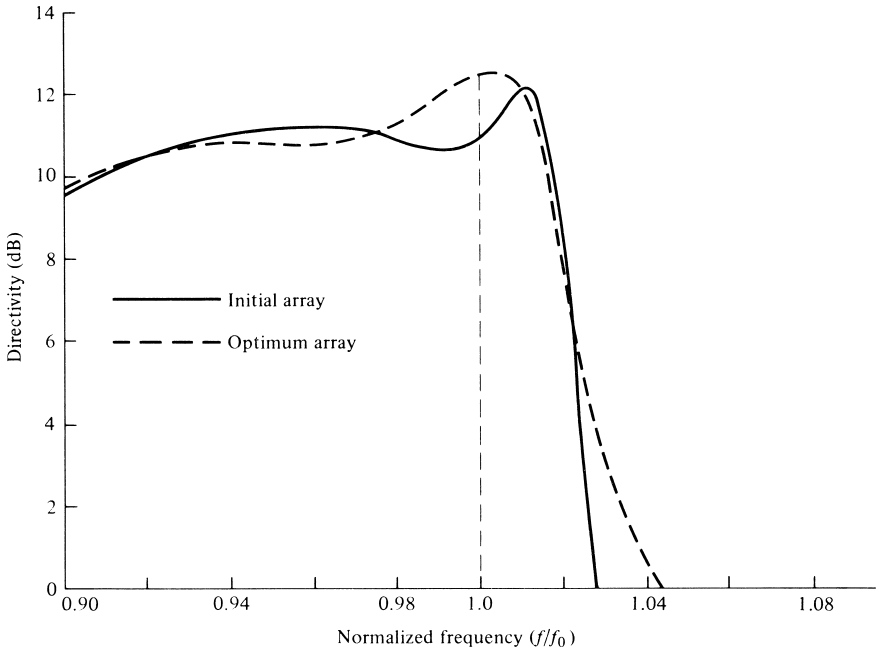

Figure 10.26 Bandwidth of initial and optimum six-element Yagi-Uda array with perturbation of all element spacings (Table 10.2). (SOURCE: N. K. Takla and L.-C. Shen, "Bandwidth of a Yagi Array with Optimum Directivity," *IEEE Trans. Antennas Propagat.*, Vol. AP-25, pp. 913–914, November 1977. © (1977) IEEE).

TABLE 10.5 Input Impedance of a 15-Element Yagi-Uda Array (Reflector Length = 0.5λ; Director Spacing = 0.34λ; Director Length = 0.406λ)

Reflector Spacing (s_{21}/λ)	Input Impedance (ohms)
0.25	62
0.18	50
0.15	32
0.13	22
0.10	12

techniques are the use of the folded dipole, of Section 9.5, as a driven element and simultaneously as an impedance transformer, and the Gamma-match of Section 9.7.4. Which one of the two is used depends primarily on the transmission line from the antenna to the receiver.

The coaxial cable is now widely used as the primary transmission line for television, especially with the wide spread and use of cable TV; in fact, most television sets are already prewired with coaxial cable connections. Therefore, if the coax with a characteristic impedance of about 78 ohms is the transmission line used from the Yagi-Uda antenna to the receiver and since the input impedance of the antenna is

typically 30–70 ohms (as illustrated in Table 10.5), the Gamma-match is the most prudent matching technique to use. This has been widely used in commercial designs where a clamp is usually employed to vary the position of the short to achieve a best match.

If, however, a "twin-lead" line with a characteristic impedance of about 300 ohms is used as the transmission line from the antenna to the receiver, as was used widely some years ago, then it would be most prudent to use a folded dipole as the driven element which acts as a step-up impedance transformer of about 4:1 (4:1) when the length of the element is exactly $\lambda/2$. This technique is also widely used in commercial designs.

Another way to explain the end-fire beam formation and whether the parameters of the Yagi-Uda array are properly adjusted for optimum directivity is by drawing a vector diagram of the progressive phase delay from element to element. If the current amplitudes throughout the array are equal, the total phase delay for maximum directivity should be about 180°, as is required by the Hansen-Woodyard criteria for improved end-fire radiation. Since the currents in a Yagi-Uda array are not equal in all the elements, the phase velocity of the traveling wave along the antenna structure is not the same from element-to-element but it is always slower than the velocity of light and faster than the corresponding velocity for a Hansen-Woodyard design. For a Yagi-Uda array, the decrease in the phase velocity is a function of the increase in total array length.

In general then, the phase velocity, and in turn the phase shift, of a traveling wave in a Yagi-Uda array structure is controlled by the geometrical dimensions of the array and its elements, and it is not uniform from element to element.

F. Design Procedure

A government document [31] has been published which provides extensive data of experimental investigations carried out by the National Bureau of Standards to determine how parasitic element diameter, element length, spacings between elements, supporting booms of different cross-sectional areas, various reflectors, and overall length affect the measured gain. Numerous graphical data is included to facilitate the design of different length antennas to yield maximum gain. In addition, design criteria are presented for stacking Yagi-Uda arrays either one above the other or side by side. A step-by-step design procedure has been established in determining the geometrical parameters of a Yagi-Uda array for a desired directivity (over that of a $\lambda/2$ dipole mounted at the same height above ground). The included graphs can only be used to design arrays with overall lengths (*from reflector element to last director*) of 0.4, 0.8, 1.2, 2.2, 3.2, and 4.2λ with corresponding directivities of 7.1, 9.2, 10.2, 12.25, 13.4, and 14.2 dB, respectively, and with a diameter-to-wavelength ratio of $0.001 \leq d/\lambda \leq 0.04$. Although the graphs do not cover all possible designs, they do accommodate most practical requests. The driven element used to derive the data was a $\lambda/2$ folded dipole, and the measurements were carried out at $f = 400$ MHz. To make the reader aware of the procedure, it will be outlined by the use of an example. The procedure is identical for all other designs at frequencies where included data can accommodate the specifications.

The basis of the design is the data included in

1. Table 10.6 which represents optimized antenna parameters for six different lengths and for a $d/\lambda = 0.0085$
2. Figure 10.27 which represents *uncompensated* director and reflector lengths for $0.001 \leq d/\lambda \leq 0.04$

TABLE 10.6 Optimized Uncompensated Lengths of Parasitic Elements for Yagi-Uda Antennas of Six Different Lengths

$d/\lambda = 0.0085$		Length of Yagi-Uda (in wavelengths)					
$s_{12} = 0.2\lambda$		**0.4**	**0.8**	**1.20**	**2.2**	**3.2**	**4.2**
LENGTH OF REFLECTOR (l_1/λ)		**0.482**	**0.482**	**0.482**	**0.482**	**0.482**	**0.475**
LENGTH OF DIRECTORS, λ	l_3	0.442	0.428	0.428	0.432	0.428	0.424
	l_4		0.424	0.420	0.415	0.420	0.424
	l_5		0.428	0.420	0.407	0.407	0.420
	l_6			0.428	0.398	0.398	0.407
	l_7				0.390	0.394	0.403
	l_8				0.390	0.390	0.398
	l_9				0.390	0.386	0.394
	l_{10}				0.390	0.386	0.390
	l_{11}				0.398	0.386	0.390
	l_{12}				0.407	0.386	0.390
	l_{13}					0.386	0.390
	l_{14}					0.386	0.390
	l_{15}					0.386	0.390
	l_{16}					0.386	
	l_{17}					0.386	
SPACING BETWEEN DIRECTORS (s_{ik}/λ)		0.20	0.20	0.25	0.20	0.20	0.308
DIRECTIVITY RELATIVE TO HALF-WAVE DIPOLE (dB)		7.1	9.2	10.2	12.25	13.4	14.2
DESIGN CURVE (SEE FIGURE 10.27)		(*A*)	(*B*)	(*B*)	(*C*)	(*B*)	(*D*)

(SOURCE: Peter P. Viezbicke, *Yagi Antenna Design*, NBS Technical Note 688, December 1976).

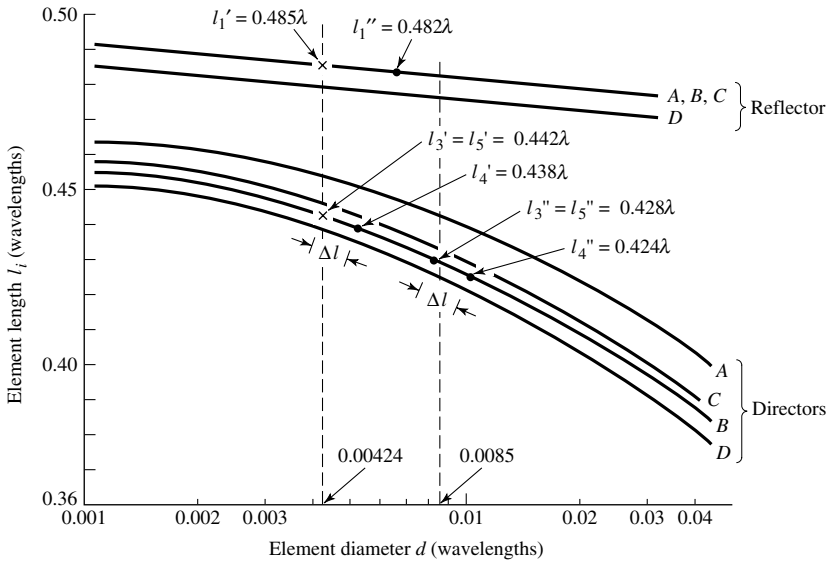

Figure 10.27 Design curves to determine element lengths of Yagi-Uda arrays. (SOURCE: P. P. Viezbicke, "Yagi Antenna Design," NBS Technical Note 688, U.S. Department of Commerce/National Bureau of Standards, December 1976).

3. Figure 10.28 which provides compensation length increase for all the parasitic elements (directors and reflectors) as a function of boom-to-wavelength ratio $0.001 \leq D/\lambda \leq 0.04$

The specified information is usually the center frequency, antenna directivity, d/λ and D/λ ratios, and it is required to find the optimum parasitic element lengths (directors and reflectors). The spacing between the directors is uniform but not the same for all designs. However, there is only one reflector and its spacing is $s = 0.2\lambda$ for all designs.

Example 10.3

Design a Yagi-Uda array with a directivity (relative to a $\lambda/2$ dipole at the same height above ground) of 9.2 dB at $f_0 = 50.1$ MHz. The desired diameter of the parasitic elements is 2.54 cm and of the metal supporting boom 5.1 cm. Find the element spacings, lengths, and total array length.

Solution:

a. At $f_0 = 50.1$ MHz the wavelength is $\lambda = 5.988$ m $= 598.8$ cm. Thus $d/\lambda = 2.54/598.8 = 4.24 \times 10^{-3}$ and $D/\lambda = 5.1/598.8 = 8.52 \times 10^{-3}$.

b. From Table 10.6, the desired array would have a total of five elements (three directors, one reflector, one feeder). For a $d/\lambda = 0.0085$ ratio the optimum uncompensated lengths would be those shown in the second column of Table 10.6 ($l_3 = l_5 = 0.428\lambda$, $l_4 = 0.424\lambda$, and $l_1 = 0.482\lambda$). The overall

antenna length would be $L = (0.6 + 0.2)\lambda = 0.8\lambda$, the spacing between directors 0.2λ, and the reflector spacing 0.2λ. It is now desired to find the optimum lengths of the parasitic elements for a $d/\lambda = 0.00424$.

c. Plot the optimized lengths from Table 10.6 ($l_3'' = l_5'' = 0.428\lambda, l_4'' = 0.424\lambda$, and $l_1'' = 0.482\lambda$) on Figure 10.27 and mark them by a dot ($\cdot$).

d. In Figure 10.27 draw a vertical line through $d/\lambda = 0.00424$ intersecting curves (B) at director uncompensated lengths $l_3' = l_5' = 0.442\lambda$ and reflector length $l_1' = 0.485\lambda$. Mark these points by an x.

e. With a divider, measure the distance (Δl) along director curve (B) between points $l_3'' = l_5'' = 0.428\lambda$ and $l_4'' = 0.424\lambda$. Transpose this distance from the point $l_3' = l_5' = 0.442\lambda$ on curve (B), established in step (d) and marked by an x, downward along the curve and determine the uncompensated length $l_4' = 0.438\lambda$. Thus the boom uncompensated lengths of the array at $f_0 =$ 50.1 MHz are

$$l_3' = l_5' = 0.442\lambda$$

$$l_4' = 0.438\lambda$$

$$l_1' = 0.485\lambda$$

f. Correct the element lengths to compensate for the boom diameter. From Figure 10.28, a boom diameter-to-wavelength ratio of 0.00852 requires a fractional length increase in each element of about 0.005λ. Thus the final lengths of the elements should be

$$l_3 = l_5 = (0.442 + 0.005)\lambda = 0.447\lambda$$

$$l_4 = (0.438 + 0.005)\lambda = 0.443\lambda$$

$$l_1 = (0.485 + 0.005)\lambda = 0.490\lambda$$

The design data were derived from measurements carried out on a nonconducting Plexiglas boom mounted 3λ above the ground. The driven element was a $\lambda/2$ folded dipole matched to a 50-ohm line by a double-stub tuner. All parasitic elements were constructed from aluminum tubing. Using Plexiglas booms, the data were repeatable and represented the same values as air-dielectric booms. However that was not the case for wooden booms because of differences in the moisture, which had a direct affect on the gain. Data on metal booms was also repeatable provided the element lengths were increased to compensate for the metal boom structure.

A commercial Yagi-Uda antenna is shown in Figure 10.29. It is a TV antenna designed primarily for channels 2–13. Its gain (over a dipole) ranges from 4.4 dB for channel 2 to 7.3 dB for channel 13, and it is designed for 300 ohms impedance.

10.3.4 Yagi-Uda Array of Loops

Aside from the dipole, the loop antenna is one of the most basic antenna elements. The pattern of a very small loop is similar to that of a very small dipole and in

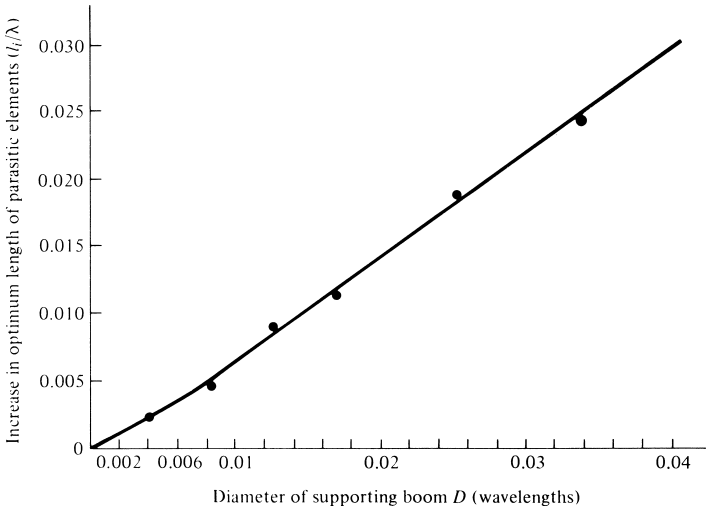

Figure 10.28 Increase in optimum length of parasitic elements as a function of metal boom diameter. (SOURCE: P. P. Viezbicke, "Yagi Antenna Design," NBS Technical Note 688, U.S. Department of Commerce/National Bureau of Standards, December 1976).

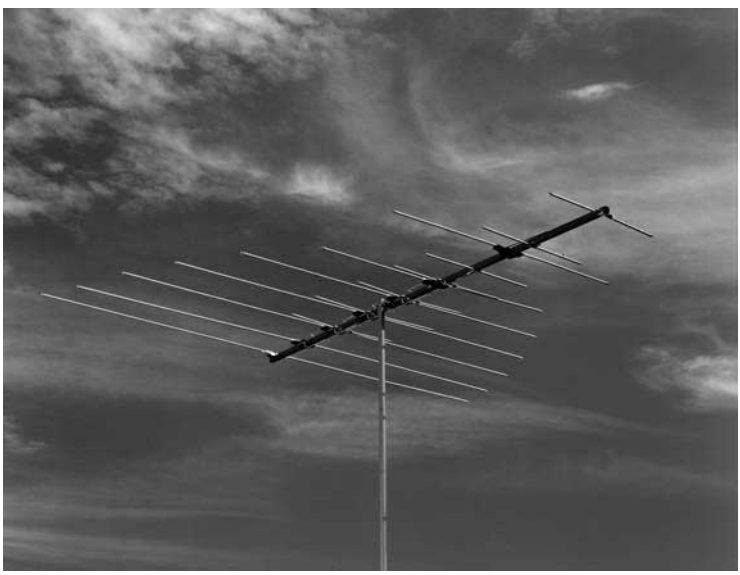

Figure 10.29 Commercial Yagi-Uda dipole TV array. (Courtesy: Winegard Company, Burlington, IA).

the far-field region it has a null along its axis. As the circumference of the loop increases, the radiation along its axis increases and reaches near maximum at about one wavelength [32]. Thus loops can be used as the basic elements, instead of the linear dipoles, to form a Yagi-Uda array as shown in Figure 10.30. By properly choosing the dimensions of the loops and their spacing, they can form a unidirectional beam along the axis of the loops and the array.

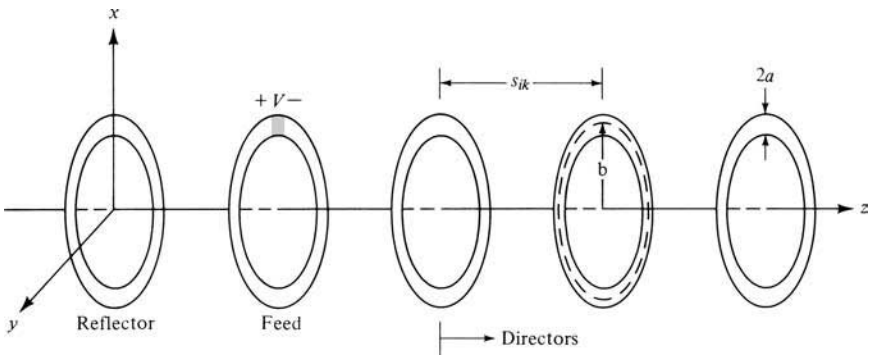

Figure 10.30 Yagi-Uda array of circular loops.

It has been shown that the radiation characteristics of a two-element loop array, one driven element and a parasitic reflector, resulted in the elimination of corona problems at high altitudes [33]. In addition, the radiation characteristics of loop arrays mounted above ground are less affected by the electrical properties of the soil, as compared with those of dipoles [34]. A two-element loop array also resulted in a 1.8 dB higher gain than a corresponding array of two dipoles [33]. A two-element array of square loops (a feeder and a reflector) in a boxlike construction is called a "cubical quad" or simply a "quad" antenna, and it is very popular in amateur radio applications [35]. The sides of each square loop are $\lambda/4$ (perimeter of λ), and the loops are usually supported by a fiberglass or bamboo cross-arm assembly.

The general performance of a loop Yagi-Uda array is controlled by the same geometrical parameters (reflector, feeder, and director sizes, and spacing between elements), and it is influenced in the same manner as an array of dipoles [36]–[38].

In a numerical parametric study of coaxial Yagi-Uda arrays of circular loops [37] of 2 to 10 directors, it has been found that the optimum parameters for *maximum forward gain* were

1. circumference of feeder $2\pi b_2 \simeq 1.1\lambda$, where b_2 is its radius. This radius was chosen so that the input impedance for an isolated element is purely resistive.
2. circumference of the reflector $2\pi b_1 \simeq 1.05\lambda$, where b_1 is its radius. The size of the reflector does not strongly influence the forward gain but has a major effect on the backward gain and input impedance.
3. feeder–reflector spacing of about 0.1λ. Because it has negligible effect on the forward gain, it can be used to control the backward gain and/or the input impedance.
4. circumference of directors $2\pi b \simeq 0.7\lambda$, where b is the radius of any director and it was chosen to be the same for all. When the circumference approached a value of one wavelength, the array exhibited its cutoff properties.
5. spacing of directors of about 0.25λ, and it was uniform for all.

The radius a of all the elements was retained constant and was chosen to satisfy $\Omega = 2\ln(2\pi b_2/a) = 11$ where b_2 is the radius of the feeder.

While most of the Yagi-Uda designs have been implemented using dipoles, and some using loops, as the primary elements, there have been Yagi-Uda designs using slots [39]

and microstrip patch elements [40]. The microstrip design was primarily configured for low-angle satellite reception for mobile communications [40].

10.4 MULTIMEDIA

In the CD that is part of the book the following multimedia resources are included for the review, understanding, and visualization of the material of this chapter:

a. **Java**-based **interactive questionnaire**, with answers.
b. **Matlab** computer programs, designated
   - ***Beverage***
   - ***Helix***

   for computing and displaying the radiation characteristics of beverage and helical antennas.
c. **Matlab** and **Fortran** computer program, designated ***Yagi_Uda***, for computing and displaying the radiation characteristics of a Yagi-Uda array design.
d. **Power Point (PPT)** viewgraphs, in multicolor.

REFERENCES

1. C. H. Walter, *Traveling Wave Antennas*, McGraw-Hill, New York, 1965.
2. J. D. Kraus, *Electromagnetics*, McGraw-Hill Book Co., New York, 1992.
3. J. G. Brainerd et al., *Ultra-High-Frequency Techniques*, Van Nostrand, New York, 1942.
4. L. V. Blake, *Antennas*, John Wiley and Sons, New York, 1966.
5. G. A. Thiele and E. P. Ekelman, Jr., "Design Formulas for Vee Dipoles," *IEEE Trans. Antennas Propagat.*, Vol. AP-28, No. 4, pp. 588–590, July 1980.
6. W. L. Weeks, *Antenna Engineering*, McGraw-Hill, New York, 1968, pp. 140–142.
7. D. G. Fink (ed.), *Electronics Engineers' Handbook*, Chapter 18 (by W. F. Croswell), McGraw-Hill, New York, 1975.
8. J. D. Kraus, *Antennas*, McGraw-Hill, New York, 1988.
9. A. A. de Carvallo, "On the Design of Some Rhombic Antenna Arrays," *IRE Trans. Antennas Propagat.*, Vol. AP-7, No. 1, pp. 39–46, January 1959.
10. E. Bruce, A. C. Beck, and L. R. Lowry, "Horizontal Rhombic Antennas," *Proc. IRE*, Vol. 23, pp. 24–26, January 1935.
11. R. S. Elliott, *Antenna Theory and Design*, Prentice-Hall, Englewood Cliffs, New Jersey, 1981.
12. J. D. Kraus, "A 50-Ohm Input Impedance for Helical Beam Antennas," *IEEE Trans. Antennas Propagat.*, Vol. AP-25, No. 6, p. 913, November 1977.
13. A. G. Kandoian, "Three New Antenna Types and Their Applications," *Proc. IRE*, Vol. 34, pp. 70W–75W, February 1946.
14. S. Uda, "Wireless Beam of Short Electric Waves," *J. IEE (Japan)*, pp. 273–282, March 1926, and pp. 1209–1219, November 1927.
15. H. Yagi, "Beam Transmission of Ultra Short Waves," *Proc. IRE*, Vol. 26, pp. 715–741, June 1928. Also *Proc. IEEE*, Vol. 72, No. 5, pp. 634–645, May 1984; *Proc. IEEE*, Vol. 85, No. 11, pp. 1864–1874, November 1997.